Effects of Wavefunction Modulation on Electron Transport in Ultrathin-Body DG MOSFETs

Nobuya Mori and Hideki Minari
Division of Electrical, Electronic and Information Engineering
Graduate School of Engineering, Osaka University
2–1 Yamada-oka, Suita City, Osaka 565-0871, Japan
Email: nobuya.mori@eei.eng.osaka-u.ac.jp

***Abstract*—Current-voltage characteristics of ultrathin-body double-gate MOSFETs are calculated within non-equilibrium Green's function formalism including g-type, f-type, and acoustic phonon scattering. By comparing results under asymmetric and symmetric bias conditions, wavefunction modulation effects on transport characteristics are investigated. On-current reduction ratio under symmetric bias condition becomes significantly smaller than that under asymmetric bias condition when silicon-body thickness $t \gtrsim 3\,\mathrm{nm}$.**

***Keywords*—MOSFET; NEGF; phonon scattering**

I. Introduction

A channel length of silicon metal-oxide-semiconductor field-effect transistors (MOSFETs) continues to shrink rapidly down to a sub-100-nm regime. At this scale, the channel length is comparable to the electron mean free path, and electrons are scattered in the channel region only a few times. In such a situation, it is not well understood how scattering affects the transport characteristics [1], [2]. Energy dissipation through electron-phonon scattering is inevitable in the analysis of irreversible transport characteristics. In addition, for confined systems, such as silicon-on-insulator (SOI) structures and semiconductor quantum wells, scattering rates and transport characteristics are greatly influenced by the electronic subband structures. It has been reported that SOI MOSFETs with SOI films thinner than the inversion layers of the bulk MOSFETs can provide higher phonon-limited mobility than the bulk silicon MOSFETs [3]. Ionized impurity scattering can also be controlled by modulating the electron wavefunctions [4]. It is, therefore, very important to investigate how scattering affects transport characteristics of ultra-small devices with incorporating such wavefunction modulation effects.

In the present study, we have performed two-dimensional (2D) non-equilibrium Green's function (NEGF) simulation [5]–[7] of silicon ultrathin-body double-gate (DG) MOSFETs including g-type, f-type, and acoustic phonon scattering to investigate effects of wavefunction modulation on electron transport characteristics. In the previous study [8], we performed 2D NEGF simulation of DG MOSFETs under asymmetric bias condition, where the gate bias is applied to the top gate while the bottom gate is grounded. In the present study, we compare results under asymmetric and symmetric bias conditions (see Fig. 1). This enables us to investigate wavefunction modulation effects on transport characteristics.

II. Method

Figure 1 illustrates a schematic diagram of the DG MOSFET structure simulated in the present study. We define the x- and z-direction as the source-to-drain transport and gate confinement direction, respectively. The gate length is $L_\mathrm{g} = 20\,\mathrm{nm}$ and the silicon-body thickness, t, is varied from $1\,\mathrm{nm}$ to $10\,\mathrm{nm}$. The thickness of SiO_2 insulators is $t_\mathrm{ox} = 0.5\,\mathrm{nm}$ [9]. The sheet doping concentration in the source and drain regions is $N_\mathrm{d} \times t = 1 \times 10^{14}\,\mathrm{cm}^{-2}$. The metal gate is assumed to have the same Fermi level as that in the source and drain regions. We consider (i) asymmetric bias condition, in which V_g is applied to the top gate while the bottom gate is grounded, and (ii) symmetric bias condition, in which $\frac{1}{2}V_\mathrm{g}$ is applied equally to the top and bottom gates. We adopted the NEGF method [5]–[7] to evaluate the source-to-drain current. The coupled eigen-mode expansion method

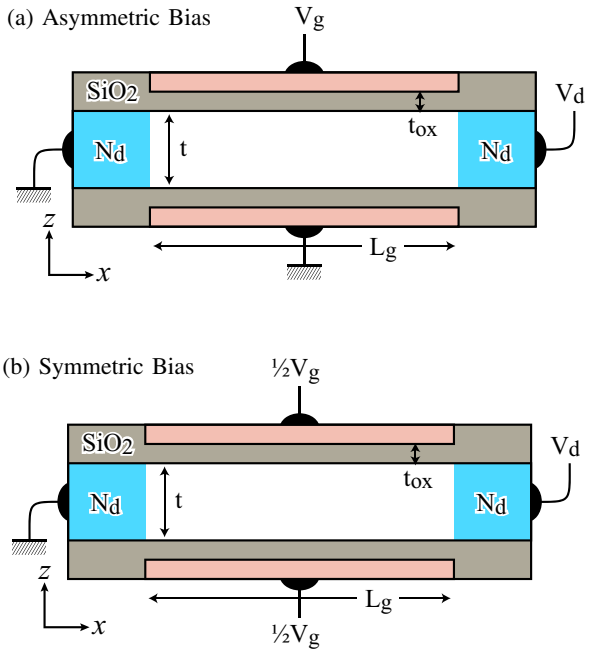

Fig. 1. Schematic diagram of the DG MOSFET structure. (a) Under asymmetric bias, the gate voltage, V_g, is applied to the top gate while the bottom gate is grounded. (b) Under symmetric bias, $\frac{1}{2}V_\mathrm{g}$ is applied equally to the top and bottom gates.

978-1-4244-1753-7/08/$25.00 ©2008 IEEE

[10]–[14] is adopted for solving the NEGF transport equation. Along the y-direction, the system is assumed to be uniform and the periodic boundary condition is applied. A discrete lattice of x_i ($i = 1, 2, \cdots, N$) is used along the x-direction and Schrödinger-like equation along the z-direction

$$\left[-\frac{\hbar^2}{2}\frac{\mathrm{d}}{\mathrm{d}z}\frac{1}{m_z}\frac{\mathrm{d}}{\mathrm{d}z} + V(x_i, z)\right]\psi_m(x_i, z) = E_m(x_i)\psi_m(x_i, z), \quad (1)$$

is solved at every x-mesh point, x_i. Here m_z is the electron effective mass along the z-direction, $V(x, z)$ is the 2D potential profile, and m is a mode index. Using the obtained subband energies, $E_m(x_i)$, and eigen-mode functions, $\psi_m(x_i, z)$, we expand the Green's function in (i, m, k_y)-space and solve the one-dimensional transport equation along the transport direction [14]. The conduction band is expressed in terms of six elliptic valleys within an effective mass approximation. We use the bulk effective masses in the present calculation.

Acoustic phonon, g-type phonon, and f-type phonon scattering are included [8]. For g-type and f-type phonons, in/out-scattering functions [5] are given by

$$\begin{aligned}\Sigma_{\mathrm{ph}}^{\mathrm{in/out}}(\lambda, \lambda'; E) &= \sum_{\nu,\boldsymbol{q}}\sum_{\lambda_1,\lambda_2} |U_\nu|^2 \langle\lambda|\mathrm{e}^{i\boldsymbol{q}\cdot\boldsymbol{r}}|\lambda_1\rangle\langle\lambda_2|\mathrm{e}^{-i\boldsymbol{q}\cdot\boldsymbol{r}}|\lambda'\rangle \\ &\times\Big[N_\nu \mathrm{G}^{\mathrm{n/p}}(\lambda_1, \lambda_2; E \mp \hbar\omega_\nu) \\ &\quad + (N_\nu + 1)\,\mathrm{G}^{\mathrm{n/p}}(\lambda_1, \lambda_2; E \pm \hbar\omega_\nu)\Big], \quad (2)\end{aligned}$$

where λ specifies the basis states of electrons, ν denotes the phonon modes, $\hbar\omega_\nu$ is the phonon energy, $N_\nu = 1/[\exp(\hbar\omega_\nu/kT) - 1]$, U_ν is the interaction potential, and G^{n} (G^{p}) is the electron (hole) correlation function. The wave-function modulation affects the scattering strength through the form factor, $\langle\lambda|\mathrm{e}^{i\boldsymbol{q}\cdot\boldsymbol{r}}|\lambda_1\rangle\langle\lambda_2|\mathrm{e}^{-i\boldsymbol{q}\cdot\boldsymbol{r}}|\lambda'\rangle$. For acoustic phonons, the in/out-scattering functions can be written in a similar form when one adopt the equipartition approximation. We use the phonon-scattering parameters in Refs. [15] and [16].

In order to obtain a self-consistent solution, 2D Poisson equation is solved self-consistently with the transport equation. To accelerate the convergence of the iterative solution, we adopt the Anderson mixing [17] and the Newton method [18].

III. Results and Discussion

A. *Ballistic condition*

Figure 2 shows drain-current–gate-voltage (I_{d}-V_{g}) characteristics in the ballistic condition under the asymmetric and symmetric bias conditions for the silicon-body thickness $t = 2\,\mathrm{nm}$ and $t = 4\,\mathrm{nm}$. For $t = 2\,\mathrm{nm}$, the size quantization along the z-direction dominates and I_{d}-V_{g} characteristics under the asymmetric and symmetric bias conditions are nearly identical. As shown in Fig. 3, however, the electron distribution profiles along the z-direction become different when $t = 4\,\mathrm{nm}$, which causes the difference in the ballistic I_{d}-V_{g} characteristics of the asymmetric and symmetric bias conditions for $t = 4\,\mathrm{nm}$ (see Fig. 2). Electrons are distributed almost uniformly along the z-direction for the symmetric bias, while electrons in the channel region are confined near the top-oxide–semiconductor interface for the asymmetric bias.

In order to see the difference in the density distribution more clearly, we plot the density distribution along the z-direction at the middle of the device ($x = 10\,\mathrm{nm}$) at $V_{\mathrm{g}} = 0.8\,\mathrm{V}$ (on-state) and $V_{\mathrm{d}} = 0.5\,\mathrm{V}$ for $t = 2$, 4, 6, 8, and 10 nm (see Fig. 4). For $t = 2\,\mathrm{nm}$, the size quantization dominates and the electron distribution is nearly symmetric with respect to the center of the silicon body in spite of the bias conditions. However, for $t \gtrsim 3\,\mathrm{nm}$, electrons are confined mainly by a triangular potential under the asymmetric bias condition, while electrons are confined by a well-like potential under the symmetric bias condition. As a result, the electron distribution along the z-direction is almost independent of the silicon-body thickness when $t \gtrsim 3\,\mathrm{nm}$ under the asymmetric bias, while

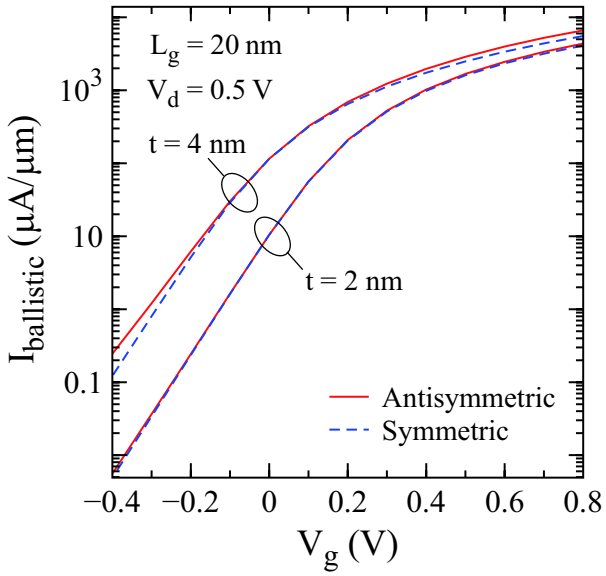

Fig. 2. Ballistic I_{d}-V_{g} characteristics for $t = 2\,\mathrm{nm}$ and $t = 4\,\mathrm{nm}$ under the asymmetric (solid lines) and the symmetric bias (dashed lines) at $V_{\mathrm{d}} = 0.5\,\mathrm{V}$ and $T = 300\,\mathrm{K}$.

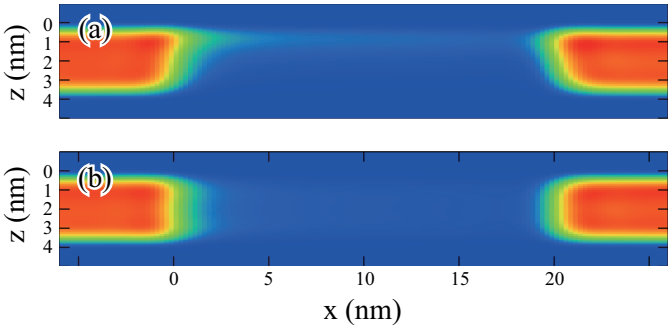

Fig. 3. Electron density in (x, z)-space in the ballistic condition at $V_{\mathrm{g}} = 0.8\,\mathrm{V}$ (on-state) and $V_{\mathrm{d}} = 0.5\,\mathrm{V}$ under the asymmetric (a) and the symmetric bias (b) for $t = 4\,\mathrm{nm}$.

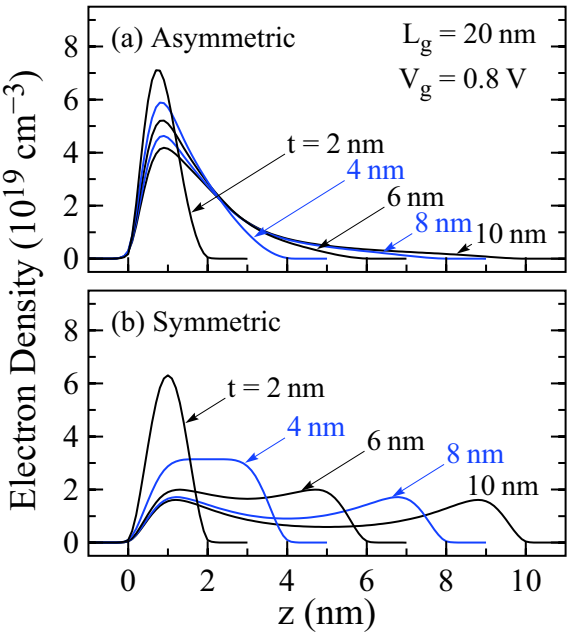

Fig. 4. Electron density along the confining direction (z-direction) at the middle of the device ($x = 10\,\mathrm{nm}$) at $V_g = 0.8\,\mathrm{V}$ (on-state) and $V_d = 0.5\,\mathrm{V}$ for $t = 2$, 4, 6, 8, and 10 nm.

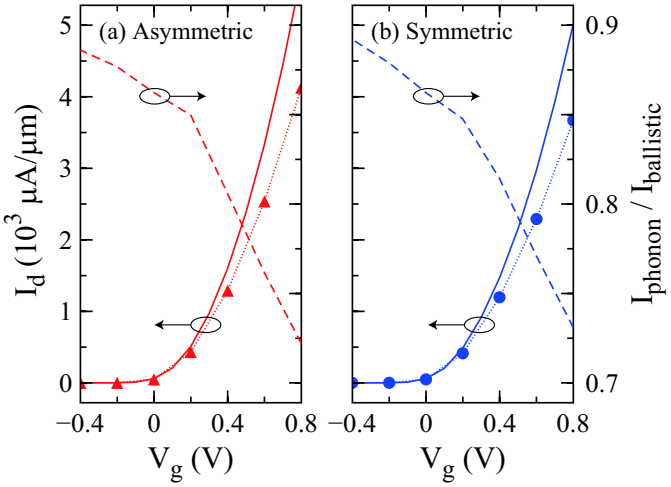

Fig. 5. I_d-V_g characteristics of the DG MOSFET with $t = 3\,\mathrm{nm}$ at $V_d = 0.5\,\mathrm{V}$. Solid lines shows I_d-V_g curves in the ballistic condition and marks are those with the phonon scattering. The current ratio, $I_{phonon}/I_{ballistic}$, is plotted by dashed lines, where I_{phonon} is the drain current with phonon scattering and $I_{ballistic}$ is that without phonon scattering.

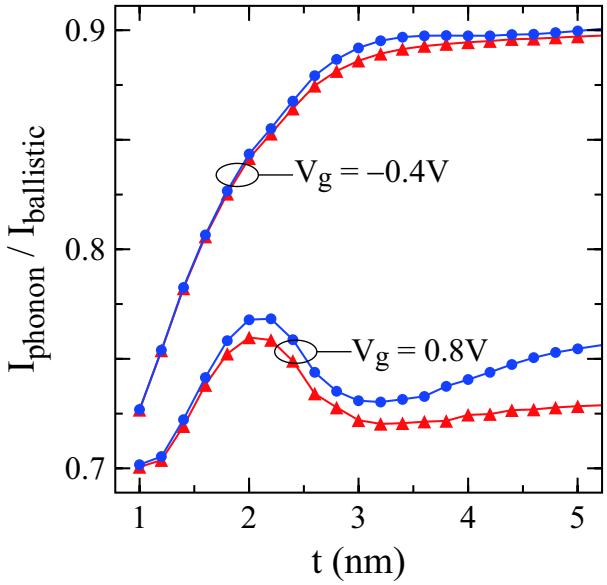

Fig. 6. Current ratio, $I_{phonon}/I_{ballistic}$, as a function of the silicon-body thickness, t, under the asymmetric (solid triangles) and the symmetric bias (solid circles) for $V_g = 0.8\,\mathrm{V}$ (on-state) and $-0.4\,\mathrm{V}$ (off-state).

electrons are almost uniformly distributed in the silicon body when $t \gtrsim 3\,\mathrm{nm}$ under the symmetric bias.

B. Effects of phonon scattering

The difference in the density distribution for $t \gtrsim 3\,\mathrm{nm}$ is originated in the difference in the electron wavefunctions associated with the quantized z-motion. This also causes different phonon-scattering strength between the asymmetric and symmetric bias conditions.

Figure 5 shows I_d-V_g characteristics of the DG MOSFET with phonon scattering and without phonon scattering, and the current ratio, $I_{phonon}/I_{ballistic}$, for $t = 3\,\mathrm{nm}$ at $V_d = 0.5\,\mathrm{V}$. Here I_{phonon} is the drain current with phonon scattering and $I_{ballistic}$ is that without phonon scattering (ballistic condition). The ratio, $I_{phonon}/I_{ballistic}$, can be, therefore, considered as a measure of how the phonon-scattering affects the current. For both bias conditions, the current reduction ratio, $\Delta I/I_{ballistic} \equiv 1 - I_{phonon}/I_{ballistic}$, of off-state is smaller than that of on-state. One can classify the drain current into classical and direct-tunneling current. The classical (direct-tunneling) current is defined to flow above (below) the potential maximum. Phonon scattering reduces the classical component, while phonon-assisted tunneling enhances the direct-tunneling component. The direct tunneling current dominates the off-current and we can expect that phonon-assisted tunneling partially compensates a current loss due to scattering [19]. This results in the smaller current reduction ratio at off-state.

Figure 6 shows current ratio, $I_{phonon}/I_{ballistic}$, as a function of the silicon-body thickness, t, under the asymmetric and symmetric bias conditions for $V_g = 0.8\,\mathrm{V}$ (on-state) and $-0.4\,\mathrm{V}$ (off-state). When $t \lesssim 2\,\mathrm{nm}$, the current ratio monotonously decreases with decreasing t for both on-state and off-state. This is because that only the lowest subband contributes to the current as $t \to 0$ and the form factor (and hence the scattering strength) for intra-subband scattering is inversely proportional to the body-thickness. When $2\,\mathrm{nm} \lesssim t \lesssim 3\,\mathrm{nm}$, the current ratio of on-state increases with decreasing t. In this region, the inter-subband scattering from the lowest two-fold valley becomes weaker when t decreases [3], resulting in increase in the current ratio with decreasing t. The difference in the current ratio between the asymmetric and symmetric

bias conditions becomes significant when $t \gtrsim 3\,\mathrm{nm}$ at on-state. Under the asymmetric bias at on-state, electrons are confined mainly by the gate electric field for $t \gtrsim 3\,\mathrm{nm}$ and the electron distribution along the z-direction is almost independent of the silicon-body thickness (see Fig. 4). This results in a constant scattering rate and constant current ratio, $I_{\mathrm{phonon}}/I_{\mathrm{ballistic}}$, when $t \gtrsim 3\,\mathrm{nm}$. On the other hand, electrons are uniformly distributed under the symmetric bias for $t \gtrsim 3\,\mathrm{nm}$ and the scattering rate becomes weaker for thicker t. This causes the gradual increase of $I_{\mathrm{phonon}}/I_{\mathrm{ballistic}}$ with t under the symmetric bias at on-state.

IV. Summary

We calculated current-voltage characteristics of DG SOI MOSFETs using the NEGF method including g-type, f-type, and acoustic phonon scattering. By comparing results under the asymmetric and symmetric bias conditions, we investigated wavefunction modulation effects on transport characteristics. We find that the difference in the current ratio, $I_{\mathrm{phonon}}/I_{\mathrm{ballistic}}$, between the asymmetric and symmetric bias conditions becomes significant when $t \gtrsim 3\,\mathrm{nm}$ at on-state. This can be attributed to the fact that electrons are confined mainly by the gate electric field for $t \gtrsim 3\,\mathrm{nm}$ under the asymmetric bias at on-state while electrons are uniformly distributed under the symmetric bias.

Acknowledgment

This work was financially supported by the Semiconductor Technology Academic Research Center (STARC) and the Global COE Program "Center for Electronic Devices Innovation" (CEDI).

References

[1] N. Sano, *Appl Phys. Lett.*, **85**, 4208 (2004).
[2] N. Sano, *Phys. Rev. Lett.*, **93**, 246803 (2004).
[3] S. Takagi, J. Koga, and A. Toriumi, *Jpn. J. Appl. Phys.*, **37**, 1289 (1998).
[4] Y. Ohno, M. Tsuchiya, and H. Sakaki, *Electron. Lett.*, **29**, 375 (1993).
[5] S. Datta, *Electronic Transport in Mesoscopic Systems* (Cambridge University Press, Cambridge, 1995).
[6] H. Haug and A.-P. Jauho, *Quantum Kinetics in Transport and Optics of Semiconductors* (Springer, Berlin, 1996).
[7] M. Lundstrom and J. Guo, *Nanoscale Transistors: Device Physics, Modeling, and Simulation*, (Springer, New York, 2006).
[8] N. Mori, H. Takeda, and H. Minari, *J. Comput. Electron.*, in print.
[9] H. Tsuchiya, K. Fujii, T. Mori, and T. Miyoshi, *IEEE Trans. Electron Devices*, **53**, 2965 (2006).
[10] R. Venugopal, Z. Ren, S. Datta, and M.S. Lundstrom, *J. Appl. Phys.*, **92**, 3730 (2002).
[11] Z. Ren, R. Venugopal, S. Goasguen, S. Datta, and M.S. Lundstrom, *IEEE Trans. Electron Devices*, **50**, 1914 (2003).
[12] R. Venugopal, M. Paulsson, S. Goasguen, S. Datta, and M.S. Lundstrom, *J. Appl. Phys.*, **93**, 5613 (2003).
[13] R. Venugopal, S. Goasguen, S. Datta, and M.S. Lundstrom, *J. Appl. Phys.*, **95**, 292 (2004).
[14] H. Takeda and N. Mori, *Jpn. J. Appl. Phys.*, **44**, 2664 (2005).
[15] C. Jacoboni and L. Reggiani, *Rev. Mod. Phys.*, **55**, 645 (1983).
[16] M. Lundstrom, *Fundamentals of Carrier Transport* (Cambridge University Press, Cambridge, 2000).
[17] V. Eyert, *J. Comput. Phys.*, **124**, 271 (1996).
[18] A. Pacelli, *IEEE Trans. Electron Devices*, **44**, 1169 (1997).
[19] H. Takeda and N. Mori, *Extended Abstracts of International Conference on Solid State Devices and Materials* (Kobe, Japan, 2005) B-4-1.